

Molecular Graph Convolutions: Moving Beyond Fingerprints

Steven Kearnes

Stanford University

kearnes@stanford.edu

Kevin McCloskey

Google Inc.

mcclloskey@google.com

Marc Berndl

Google Inc.

marcberndl@google.com

Vijay Pande

Stanford University

pande@stanford.edu

Patrick Riley

Google Inc.

pfr@google.com

Abstract

Molecular “fingerprints” encoding structural information are the workhorse of cheminformatics and machine learning in drug discovery applications. However, fingerprint representations necessarily emphasize particular aspects of the molecular structure while ignoring others, rather than allowing the model to make data-driven decisions. We describe molecular *graph convolutions*, a novel machine learning architecture for learning from undirected graphs, specifically small molecules. Graph convolutions use a simple encoding of the molecular graph (atoms, bonds, distances, etc.), allowing the model to take greater advantage of information in the graph structure.

1 Introduction

Computer-aided drug design requires representations of molecules that can be related to biological activity or other experimental endpoints. These representations encode structural features, physical properties, or activity in other assays (Todeschini and Consonni, 2009; Petrone et al., 2012). The recent advent of “deep learning” has enabled the use of very raw representations that are less application-specific when building machine learning models (Le-Cun et al., 2015). For instance, image recognition models that were once based on complex features extracted from images are now trained exclusively on the pixels themselves—deep architectures can “learn” appropriate representations for input data. Consequently, deep learning systems for drug screening or design should benefit from molecular representations

that are as complete and general as possible rather than relying on application-specific features or encodings.

First-year chemistry students quickly become familiar with a common representation for small molecules: the molecular graph. Figure 1 gives an example of the molecular graph for ibuprofen, an over-the-counter non-steroidal anti-inflammatory drug (NSAID). The atoms and bonds between atoms form the nodes and edges, respectively, of the graph. Both atoms and bonds have associated properties, such as atom type and bond order. Although the basic molecular graph representation does not capture the quantum mechanical structure of molecules or necessarily express all of the information that it might suggest to an expert medicinal chemist, its ubiquity in academia and industry makes it a desirable starting point for machine learning on chemical information.

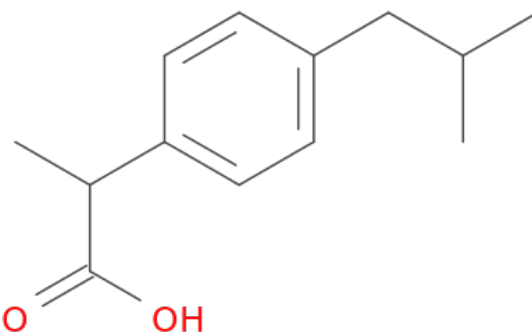


FIGURE 1: Molecular graph for ibuprofen. Unmarked vertices represent carbon atoms, and bond order is indicated by the number of lines used for each edge.

Here we describe molecular *graph convolutions*, a deep learning system using a representation of small molecules as undirected graphs of atoms. Graph convolutions extract meaningful features from simple descriptions of the graph structure—atom and bond properties, and graph distances—to form molecule-level representations that can be used in place of fingerprint descriptors in conventional machine learning applications.

2 Related Work

The history of molecular representation is extremely diverse (Todeschini and Consonni, 2009) and a full review is outside the scope of this report. Below we describe examples from several major branches of the field to provide context for our work. Additionally, we review several recent examples of graph-centric approaches in cheminformatics.

Much of cheminformatics is based on so-called “2D” molecular descriptors that attempt to capture relevant structural features derived from the molecular graph. In general, 2D features are computationally inexpensive and easy to interpret and visualize. One of the most common representations in this class is extended-connectivity fingerprints (ECFP), also referred to as circular or Morgan fingerprints (Rogers and Hahn, 2010). Starting at each heavy atom, a “bag of fragments” is constructed by iteratively expanding outward along bonds (usually the algorithm is terminated after 2–3 steps). Each unique fragment is assigned an integer identifier, which is often hashed into a fixed-length representation or “fingerprint”. Additional descriptors in this class include decompositions of the molecular graph into subtrees or fixed-length paths (GraphSim Toolkit, OpenEye Scientific Software, Inc., Santa Fe, NM, USA), as well as atom pair (AP) descriptors that encode atom types and graph distances (number of intervening bonds) for all pairs of atoms in a molecule (Carhart et al., 1985).

Many representations encode 3D information, with special emphasis on molecular shape and electrostatics as primary drivers of biological interactions in real-world systems. Pharmacophore models attempt to identify particular interactions relative to a common alignment that are critical for activity (Horvath, 2011). Rapid overlay of chemical structures (ROCS) aligns pairs of pre-generated conformers and calculates shape and electrostatic (“color”) similarity using Gaussian representations of atoms and color fea-

tures defined by a simple force field (Rush et al., 2005). ROCS can also be used to generate alignments for calculation of electrostatic field similarity (Muchmore et al., 2006). Ultrafast shape recognition (USR) calculates alignment-free 3D similarity by comparing distributions of intramolecular distances (Ballester and Richards, 2007).

Alternative approaches incorporate a broader biological context into molecular descriptions. For example, affinity fingerprints report activity in a panel of assays, allowing structurally distinct compounds to be related by similar pharmacology (Briem and Lessel, 2000; Petrone et al., 2012). The similarity ensemble approach (SEA) builds upon traditional fingerprint similarity methods for protein target identification, relating proteins by the similarity of their ligands (Keiser et al., 2007).

Other approaches from both the cheminformatics and the machine learning community directly operate on graphs in a way similar to how we do here. The “molecular graph networks” of Merkwirth and Lengauer (2005) iteratively update a state variable on each atom with learned weights specific to each atom type–bond type pair. Similarly, Micheli (2009) presents a more general formulation of the same concept of iterated local information transfer across edges and applies this method to predicting the boiling point of alkanes.

Scarselli et al. (2009) similarly defines a local operation on the graph. Rather than iterating a fixed number of times, they demonstrate that a fixed point across all the local functions can be found and defines that fixed point as the computed value for each node in the graph. In another vein, Lusci et al. (2013) convert undirected molecular graphs to a directed recursive neural net and take an ensemble over multiple conversions.

Recently, Duvenaud et al. (2015) presented an architecture trying to accomplish many of the same goals as this work. The architecture was based on generalizing the fingerprint computation such that it can be learned via backpropagation. They demonstrate that this architecture improves predictions of solubility and photovoltaic efficiency but not binding affinity.

Bruna et al. (2013) introduce convolutional deep networks on spectral representations of graphs. However, these methods apply when the graph structure is fixed across examples and only the labeling/features on individual nodes varies.

Convolutional networks on non-Euclidean mani-

folds were described by Masci et al. (2015). The problem addressed was to describe the shape of the manifold (such as the surface of a human being) in such a way that the shape descriptor of a particular point was invariant to perturbations such as movement and deformation. Unlike this and other work on molecular graphs, their goal was to have a descriptor for every point and not a descriptor for the entire shape. Therefore, the problem of how to combine all the local shape descriptors into a single descriptor was not addressed.

3 Methods

3.1 Desired invariants of a model

A primary goal of designing a deep learning architecture is to restrict the set of functions that can be learned to ones that match the desired properties from the domain. For example, in image understanding, spatial convolutions force the model to learn functions that are invariant to translation.

For a deep learning architecture taking a molecular graph as input, some arbitrary choice must be made for the order that the various atoms and bonds are presented to the model. Since that choice is arbitrary, we want:

Property 1 (Order invariance). *The output of the model should be invariant to the order that the atom and bond information is encoded in the input.*

Note that many current procedures for fingerprinting molecules achieve Property 1. We will now gradually construct an architecture which achieves Property 1 while making available a richer space of learnable parameters.

The first basic unit of representation is an *atom layer* which contains an n -dimensional vector associated with each atom. Therefore the atom layer is a 2 dimensional matrix indexed first by atom. Part of the original input will be encoded in such an atom layer and the details of how we construct the original input vector are discussed in Section 3.4. The next basic unit of representation is a *pair layer* which contains an n -dimensional vector associated with each pair of atoms. Therefore, the pair layer is a 3 dimensional matrix where the first two dimensions are indexed by atom. Note that the pair input can contain information not just about edges but about any arbitrary pair. Notably, we will encode the graph distance (length of shortest path from one atom to the

other) in the input pair layer. The order of the atom indexing for the atom and pair layer inputs must be the same.

We will describe various operations to compute new atom and pair layers with learnable parameters at every step. Notationally, let A^x be the value of a particular atom layer x and P^y be the value of a particular pair layer y . The inputs that produce those values should be clear from the context. A_a^x refers to the value of atom a in atom layer x and $P_{(a,b)}^y$ refers to the value of pair (a,b) in pair layer y .

In order to achieve Property 1 for the overall architecture, we need a different type of invariance for each atom and pair layer.

Property 2 (Atom and pair permutation invariance). *The values of an atom layer and pair permute with the original input layer order. More precisely, if the inputs are permuted with a permutation operator Q , then for all layers x, y , A^x and P^y are permuted with operator Q as well.*

In other words, Property 2 means that from a single atom’s (or pair’s) perspective, its value in every layer is invariant to the order of the other atoms (or pairs).

Since molecules are undirected graphs, we will also maintain the following:

Property 3 (Pair order invariance). *For all pair layers y , $P_{(a,b)}^y = P_{(b,a)}^y$*

Property 3 is easy to achieve at the input layer and the operations below will maintain this.

Properties 2 and 3 make it easy to construct a molecule-level representation from an atom or pair such that the molecule-level representation achieves Property 1 (see Section 3.3).

3.2 Invariant-preserving operations

We now define a series of operations that maintain the above properties.

Throughout, f represents an arbitrary function and g represents an arbitrary *commutative* function (g returns the same result regardless of the order the arguments are presented). In this work, f is a learned linear operator with a rectified linear activation function and g is a sum.

The most trivial operation is to combine one or more layers of the same type by applying the same operation to every atom or pair. Precisely, this means if you have layers x_1, x_2, \dots, x_n and function f , you can

compute a new atom layer from the previous atom layer ($A \rightarrow A$) as

$$A_a^y = f(A_a^{x1}, A_a^{x2}, \dots, A_a^{xn}) \quad (1)$$

or pair layer from the previous pair layer ($P \rightarrow P$) as

$$P_{a,b}^y = f(P_{a,b}^{x1}, P_{a,b}^{x2}, \dots, P_{a,b}^{xn}) \quad (2)$$

Since we apply the same function for every atom/pair, we refer to this as a convolution. All the transformations we develop below will have this convolution nature of applying the same operation to every atom/pair, maintaining Property 2.

When operating on pairs of atoms, instead of putting all pairs through this function, you could select a subset. In Section 4.3.3 we show experiments for restricting the set of pairs to those that are less than some graph distance away.

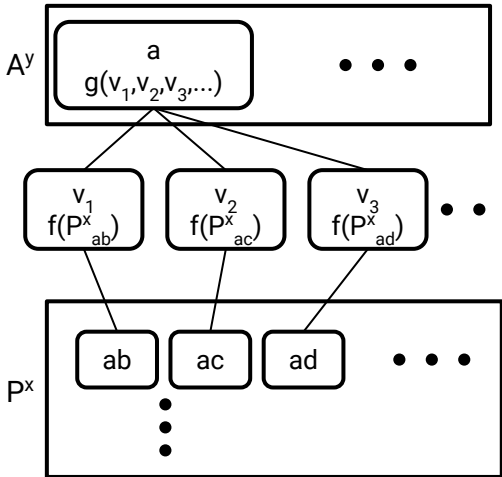


FIGURE 2: $P \rightarrow A$ operation.

Next, consider an operation that takes a pair layer x and constructs an atom layer y ($P \rightarrow A$). The operation is depicted in Figure 2. Formally:

$$A_a^y = g(f(P_{(a,b)}^x), f(P_{(a,c)}^x), f(P_{(a,d)}^x), \dots) \quad (3)$$

In other words, take all pairs of which a is a part, run them through f , and combine them with g . Note that Property 3 means we can choose an arbitrary one of $P_{(a,b)}^x$ or $P_{(b,a)}^x$.

The most interesting construction is making a pair layer from an atom layer ($A \rightarrow P$). The operation is graphically depicted in Figure 3 and formally as

$$P_{ab}^y = g(f(A_a^x, A_b^x), f(A_b^x, A_a^x)) \quad (4)$$

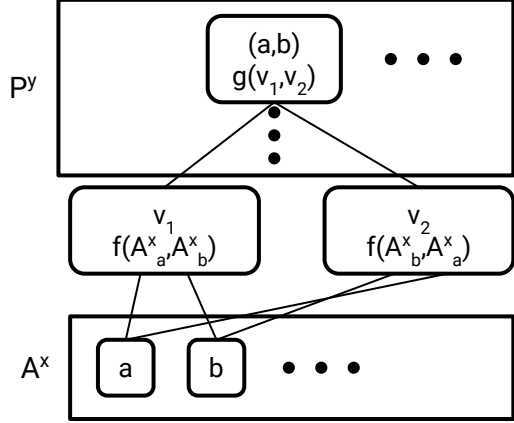


FIGURE 3: $A \rightarrow P$ operation.

Note that just applying g to A_a^x and A_b^x would maintain Properties 2 and 3 but we use this more complex form. While commutative operators (such as max pooling) are common in neural networks, commutative operators *with learnable parameters* are not common. Therefore, we use f to give learnable parameters while maintaining the desired properties.

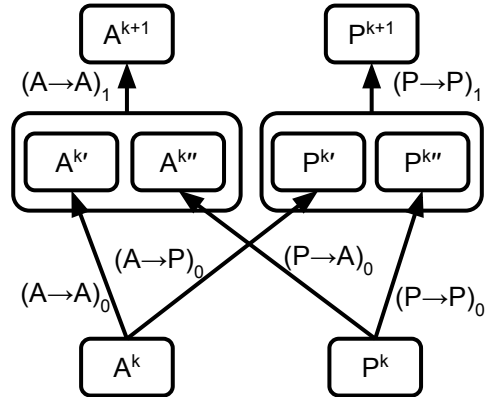


FIGURE 4: Weave module.

Once we have all the primitive operations on atom and pair layers ($A \rightarrow A$, $P \rightarrow P$, $P \rightarrow A$, $A \rightarrow P$), we can combine these into one module. We call this the Weave module (Figure 4) because the atoms and pair layers cross back and forth to each other. The module can be stacked to an arbitrary depth similar to the Inception module that inspired it (Szegedy et al., 2015).

3.3 Molecule-level features

The construction of the Weave module maintains Properties 2 and 3. What about overall order invariance (Property 1)? At the end of a stack of Weave modules we are left with an n -dimensional vector associated with every atom and an m -dimensional vector associated with every pair. We need to turn this into a molecule-level representation with some commutative function of these vectors.

In related work (Merkwirth and Lengauer, 2005; Duvenaud et al., 2015; Lusci et al., 2013), a simple unweighted sum is often used to combine order-dependent atom features into order-independent molecule-level features. However, reduction to a single value does not capture the distribution of learned features. We experimented with an alternative approach and created “fuzzy” histograms for each dimension of the feature vector.

A fuzzy histogram is described by a set of *membership functions* that are functions with range $[0, 1]$ representing the membership of the point in the bin (Zadeh, 1965). A standard histogram has membership functions which are 1 in the bin and 0 everywhere else. For each point, we normalize so that the total contribution to all bins is 1. The value of a bin in the histogram over all points is just the sum of the normalized contributions for all the points.

Figure 5 gives an example of a fuzzy histogram composed of three Gaussian bins. A histogram is built for each dimension of the feature vectors and the concatenation of those histograms is the molecule-level representation.

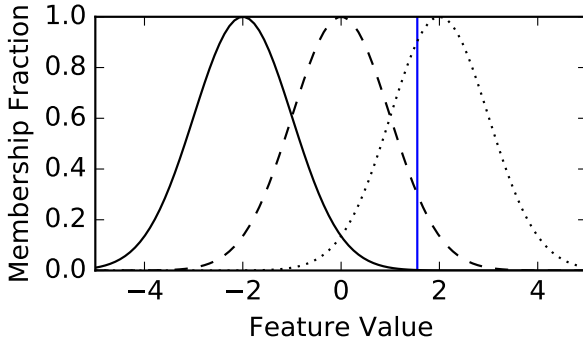


FIGURE 5: Fuzzy histogram with three Gaussian “bins”. Each curve represents the membership function for a different bin, indicating the degree to which a point contributes to that bin. The vertical blue line represents an example point which contributes normalized densities of < 0.01 , ~ 0.25 , and ~ 0.75 to the bins (from left to right).

In this work we used Gaussian membership functions (which are unnormalized versions of the standard Gaussian PDF) with eleven bins spanning a Gaussian distribution with mean of 0 and unit standard deviation, shown in Figure A10.

Throughout this paper, we construct the molecule-level features only from the top-level atom features and not the pair features. This is to restrict the total number of feature vectors that must be summarized while still providing information about the entire molecule.

Before the molecule-level featurization, we do one final convolution on the atoms. Since molecule-level featurization can be a major bottleneck in the model, this convolution expands the depth so that each dimension of the atom feature vector contains less information and therefore less information is lost during the molecule-level featurization. On this convolution, we do not use a ReLU activation function to avoid the histogram having many points at zero.

Once you have a molecule-level representation, this becomes a more standard multitask problem. We follow the common approach (Ramsundar et al., 2015; Ma et al., 2015; Unterthiner et al., 2015) of a small number of fully connected layers on top of the molecule-level features followed by standard softmax classification.

The overall architecture is depicted in Figure 6. Table 1 lists hyperparameters and default values for graph convolution models. For molecules that have more than the maximum number of atoms, only a subset of atoms (and therefore atom pairs) are represented in the input encoding. This subset depends on the order in which the atoms are traversed by the featurization code and should be considered arbitrary. In models with multiple Weave modules it is possible to vary the convolution depths in a module-specific way. However, the models in this work used the same settings for all Weave modules.

3.4 Input featurization

The initial atom and pair features are summarized in Table 2 and Table 3, respectively. The features are a mix of floating point, integer, and binary values (all encoded as floating point numbers in the network). The feature set is intended to be broad, but not necessarily exhaustive, and we recognize that some features can potentially be derived from or correlated to a subset of the others (e.g., atom hybridization can be determined by inspecting the bonds that atom makes). We performed experiments using a “simple”

TABLE 1: Graph convolution model hyperparameters.

| Group | Hyperparameter | Default Value |
|----------------|--|--------------------|
| Input | Maximum number of atoms per molecule | 60 |
| | Maximum atom pair graph distance | 2 |
| Weave | Number of Weave modules | 1 |
| | $(A \rightarrow A)_0$ convolution depth | 50 |
| | $(A \rightarrow P)_0$ convolution depth | 50 |
| | $(P \rightarrow P)_0$ convolution depth | 50 |
| | $(P \rightarrow A)_0$ convolution depth | 50 |
| | $(A \rightarrow A)_1$ convolution depth | 50 |
| | $(P \rightarrow P)_1$ convolution depth | 50 |
| | | |
| Reduction | Final atom layer convolution depth | 128 |
| | Reduction to molecule-level features | Gaussian histogram |
| Post-reduction | Fully-connected layers (number of units) | 2000, 100 |
| Training | Batch size | 96 |
| | Learning rate | 0.003 |
| | Optimization method | Adagrad |

TABLE 2: Atom features.

| Feature | Description | Size |
|------------------|---|------|
| Atom type* | H, C, N, O, F, P, S, Cl, Br, I, or metal (one-hot or null). | 11 |
| Chirality | R or S (one-hot or null). | 2 |
| Formal charge | Integer electronic charge. | 1 |
| Partial charge | Calculated partial charge. | 1 |
| Ring sizes | For each ring size (3–8), the number of rings that include this atom. | 6 |
| Hybridization | sp, sp ² , or sp ³ (one-hot or null). | 3 |
| Hydrogen bonding | Whether this atom is a hydrogen bond donor and/or acceptor (binary values). | 2 |
| Aromaticity | Whether this atom is part of an aromatic system. | 1 |
| | | 27 |

* Included in the “simple” featurization (see Section 4.2).

TABLE 3: Atom pair features.

| Feature | Description | Size |
|-----------------|---|------|
| Bond type* | Single, double, triple, or aromatic (one-hot or null). | 4 |
| Graph distance* | For each distance (1–7), whether the shortest path between the atoms in the pair is less than or equal to that number of bonds (binary values). | 7 |
| Same ring | Whether the atoms in the pair are in the same ring. | 1 |
| | 12 | |

* Included in the “simple” featurization (see Section 4.2).

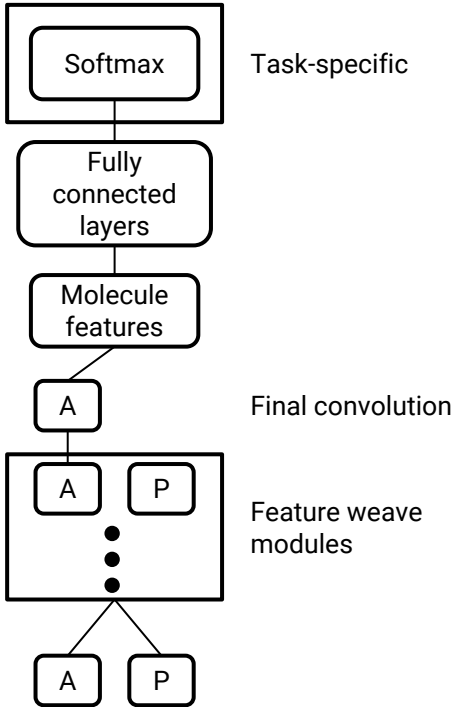


FIGURE 6: Abstract graph convolution architecture.

subset of these features in an effort to understand their relative contributions to learning (Section 4.2), but many other questions about specifics of the input featurization are left to future work.

All features were generated with RDKit (Landrum), including Gasteiger atomic partial charges (Gasteiger and Marsili, 1980). Although our featurization includes space for hydrogen atoms, we did not use explicit hydrogens in any of our experiments in order to conserve memory and emphasize contributions from heavy atoms.

Other deep learning applications with more “natural” inputs such as computer vision and speech recognition still require some input engineering; for example, adjusting images to a specific size or scale, or transforming audio into the frequency domain. Likewise, the initial values for the atom and pair layers describe these primitives in terms of properties that are often considered by medicinal chemists and other experts in the field, allowing the network to use or ignore them as needed for the task at hand. One of the purposes of this work is to demonstrate that learning can occur with as little preprocessing as possible. Accordingly, we favor simple descriptors that are more or less “obvious”.

3.5 Datasets

We used a dataset collection nearly identical to the one described by Ramsundar et al. (2015) except for some changes to the data processing pipeline (including the duplicate merging process for the Tox21 dataset) and different cross-validation fold divisions. Briefly, there are 259 datasets divided into four groups indicating their source: PubChem BioAssay (Wang et al., 2012) (PCBA, 128 datasets), the “maximum unbiased validation” datasets constructed by Rohrer and Baumann (Rohrer and Baumann, 2009) (MUV, 17 datasets), the enhanced directory of useful decoys (Mysinger et al., 2012) (DUD-E, 102 datasets), and the training set for the Tox21 challenge (Huang et al., 2015) (Tox21, 12 datasets). The combined dataset contained over 38 million data points and included targets from many different biological classes.

3.6 Model training and evaluation

Graph convolution and traditional neural network models were implemented in TensorFlow (Abadi et al., 2015), an open-source library for machine learning. Some additional features such as replicated training were not available outside of Google at the time of this work. Models were evaluated by their 5-fold mean area under the receiver operating characteristic curve (AUC).

Graph convolution models were trained for 3–8 million steps using the Adagrad optimizer (Duchi et al., 2011) with learning rate 0.003 and batch size 96, with periodic checkpointing. All convolution and fully-connected layer outputs were batch normalized (Ioffe and Szegedy, 2015) prior to applying the ReLU nonlinearity.

To establish a baseline, we also trained pyramidal multitask neural network (MTNN) (Ramsundar et al., 2015), random forest (RF), and logistic regression (LR) models using Morgan fingerprints with radius 2 (essentially equivalent to ECFP4) generated with RDKit (Landrum). The pyramidal MTNN had two hidden layers (2000 and 100 units, respectively) with rectified linear activations, and was trained for 20 million steps using the SGD optimizer with batch size 128 and a learning rate of 0.0003, with periodic checkpointing. (Training was allowed to continue to 20 million steps after we observed undertraining on the Tox21 datasets.) Additionally, this model used 0.25 dropout (Srivastava et al., 2014), initial weight standard deviations of 0.01 and 0.04 and initial biases

of 0.5 and 3.0 in the respective hidden layers. This model did not use batch normalization.

In graph convolution and pyramidal MTNN models, active compounds were weighted in the cost function such that the total active weight equalled the total inactive weight within each dataset. For evaluation, a target step (a multiple of 1000) was chosen such that the mean over all datasets (excluding DUD-E) of the 5-fold mean AUC—using the closest checkpoint to the target step in each cross-validation fold—was maximized.

Logistic regression models were trained with the `LogisticRegression` class in scikit-learn (Pedregosa et al., 2011), with uniform example weighting. Values for the `penalty` and `C` parameters were chosen by grid search. Random forest models were trained using the scikit-learn `RandomForestClassifier` with hyperparameters similar to those described by Ma et al. (2015), specifically `n_estimators`=100, `max_features`=1/3., and `min_samples_split`=6, with uniform example weighting.

4 Results

4.1 Proof of concept

With so many hyperparameters to adjust, we sought to establish a centerpoint from which to investigate specific questions. After several experiments, we settled on a simple model with two Weave modules, a maximum atom pair distance of 2, Gaussian histogram molecule-level reductions, and two fully-connected layers of size 2000 and 100, respectively. This model is listed in Table 4 as W₂N₂. Each graph convolution model in Table 4 is derived from this centerpoint by varying a single hyperparameter.

To statistically compare the graph convolution models to current state of the art, for each model (and within each dataset group) we do a sign test compared to the Pyramidal (2000, 100) MTNN or the Random Forest model. The sign test calculates the proportion of datasets that achieved a higher 5-fold mean AUC than the baseline model. In Table 4 we report a Wilson score interval for this proportion at 95% confidence. Models with intervals that do not include 0.5 are considered significantly different in their performance. To calculate these intervals, we used the `proportion_confint` function in `statsmodels` (Seabold and Perktold, 2010) version 0.6.1 with `method='wilson'` and `alpha=0.05`, counting only non-zero differences in the sign test. We do

not report values for the DUD-E datasets since all models achieved > 0.99 median 5-fold mean AUC for that dataset group.

Graph convolution models achieve comparable performance to the baseline pyramidal multitask neural network (MTNN) on the classification tasks in our dataset collection, which is a remarkable result considering the simplicity of our input representation. Notably, many of the graph convolution models significantly outperform the pyramidal MTNN and random forest baselines on the Tox21 datasets. Inspection of the training curves for the pyramidal MTNN shows that the median 5-fold mean AUC for the Tox21 datasets continues to increase throughout training, but even after 20 million steps it has not matched the graph convolution performance level (data not shown; note that the pyramidal MTNN is evaluated much earlier than 20 million steps, per the procedure described in Section 3.6).

4.2 Input featurization

As a further proof of concept and to address the importance of the initial featurization, we built a model using a subset of features that match typical 2D structural diagrams seen in chemistry textbooks: only atom type, bond type, and graph distance are provided to the network. Figure 7 compares a model built with this “simple” input featurization to a “full” featurization containing all features from Table 2 and Table 3. Both featurizations achieve similar median 5-fold mean AUC scores, although the “full” featurization appears to have less variance on the MUV datasets. This result suggests that the additional features in the “full” representation are either mostly ignored during training or can be derived from a simpler representation of the molecular graph. Further work is required to understand the importance of individual features, perhaps with datasets that are sensitive to particular components of the input representation (such as hydrogen bonding or formal charge).

Figure 8 gives examples of how the initial atom features for a single molecule (ibuprofen) evolve as they progress through graph convolution Weave modules. The initial atom and pair feature encodings for the “full” featurization are depicted in panel (A). Comparing the initial atom features to their source molecular graph, the aromatic carbons in the central ring are clearly visible (and nearly identical in the featurization). The pair features are more difficult to interpret visually, and mostly encode graph distance. As the atom features are transformed by the Weave mod-

TABLE 4: Median 5-fold mean AUC values for reported models. Graph convolution models are labeled as $W_x N_y$, where x and y denote the number of Weave modules and the maximum atom pair distance, respectively (see the text for descriptions of the simple, sum, and RMS models). All graph convolution models feed into a Pyramidal (2000, 100) MTNN after the molecule-level feature reduction step. Logistic Regression, Random Forest, and Pyramidal (2000, 100) MTNN baselines were trained using Morgan fingerprints (ECFP4) as input. For each model, we report the 95% Wilson score interval for a sign test comparing that model to the best baseline model within each dataset group (Pyramidal (2000, 100) MTNN for PCBA and MUV, Random Forest for Tox21), excluding DUD-E (see Section 3.6 and Section 4).

| Model | PCBA ($n = 128$) | | MUV ($n = 17$) | | Tox21 ($n = 12$) | |
|----------------------------|--------------------|--------------|------------------|--------------|--------------------|--------------|
| | Median | Sign Test CI | Median | Sign Test CI | Median | Sign Test CI |
| Logistic Regression | 0.845 | [0.05, 0.15] | 0.795 | [0.10, 0.47] | 0.801 | [0.01, 0.35] |
| Random Forest | 0.847 | [0.04, 0.14] | 0.764 | [0.06, 0.41] | 0.841 | |
| Pyramidal (2000, 100) MTNN | 0.915 | | 0.894 | | 0.808 | [0.01, 0.35] |
| $W_2 N_2$ -simple | 0.908 | [0.20, 0.36] | 0.875 | [0.10, 0.47] | 0.866 | [0.65, 0.99] |
| $W_2 N_2$ -sum | 0.902 | [0.19, 0.34] | 0.847 | [0.13, 0.53] | 0.854 | [0.55, 0.95] |
| $W_2 N_2$ -RMS | 0.904 | [0.13, 0.26] | 0.850 | [0.17, 0.59] | 0.863 | [0.65, 0.99] |
| $W_1 N_2$ | 0.903 | [0.10, 0.23] | 0.845 | [0.06, 0.41] | 0.856 | [0.47, 0.91] |
| $W_2 N_1$ | 0.913 | [0.25, 0.41] | 0.881 | [0.13, 0.53] | 0.870 | [0.65, 0.99] |
| $W_2 N_2$ | 0.912 | [0.33, 0.50] | 0.872 | [0.31, 0.74] | 0.871 | [0.65, 0.99] |
| $W_2 N_3$ | 0.910 | [0.34, 0.51] | 0.877 | [0.13, 0.53] | 0.864 | [0.65, 0.99] |
| $W_2 N_4$ | 0.907 | [0.24, 0.40] | 0.878 | [0.10, 0.47] | 0.861 | [0.65, 0.99] |
| $W_2 N_\infty$ | 0.904 | [0.12, 0.26] | 0.856 | [0.13, 0.53] | 0.853 | [0.55, 0.95] |
| $W_3 N_2$ | 0.912 | [0.27, 0.44] | 0.874 | [0.22, 0.64] | 0.859 | [0.55, 0.95] |
| $W_4 N_2$ | 0.910 | [0.33, 0.49] | 0.865 | [0.22, 0.64] | 0.866 | [0.65, 0.99] |

ules (panel (B)), they become more heterogeneous and reflective of their unique chemical environments. “Simple” features behave similarly, beginning with rather sterile initial values and quickly diverging as neighborhood information is included by Weave module operations (panel (C)). Comparison of the “full” and “simple” atom features after the second Weave module shows that both featurizations lead to qualitatively similar feature distributions. Figure A8 and Figure A9 show similar behavior for pair features.

4.3 Hyperparameter sensitivity

4.3.1 Number of Weave modules

In relatively “local” models with limited atom pair distance, successive Weave modules update atom features with information from progressively larger regions of the molecule. This suggests that the number of Weave modules is a critical hyperparameter to optimize, analogous to the number of hidden layers in traditional neural networks. Figure 9 compares models with 2–4 Weave modules to a model with a single Weave module. As expected, models with a single Weave layer are outperformed by deeper architectures. However, there does not appear to be

much benefit to using more than two Weave modules (at least for our datasets), especially when the added cost of training a deeper model is considered.

4.3.2 Alternative feature reductions

The reduction of atom features from the final Weave module to an order-invariant, molecule-level representation is a major information bottleneck in graph convolution models. In related work, a simple unweighted sum (Duvenaud et al., 2015; Merkwirth and Lengauer, 2005; Lusci et al., 2013) or root-mean-square (Dieleman, March 17, 2015) (RMS) reduction is used. Using a consistent base architecture with two Weave modules and a maximum atom pair distance of 2 (see Section 4.3.3), we compared these traditional reductions with our Gaussian histogram approach. Models using the RMS reduction were somewhat unstable in terms of mean non-DUDE 5-fold mean AUC during training (data not shown), and it was not clear that these models had fully converged when they were evaluated (after ~ 4.5 million steps).

Gaussian histogram models have higher median 5-fold mean AUC values in each dataset group (Figure A6) and improved scores relative to both sum and

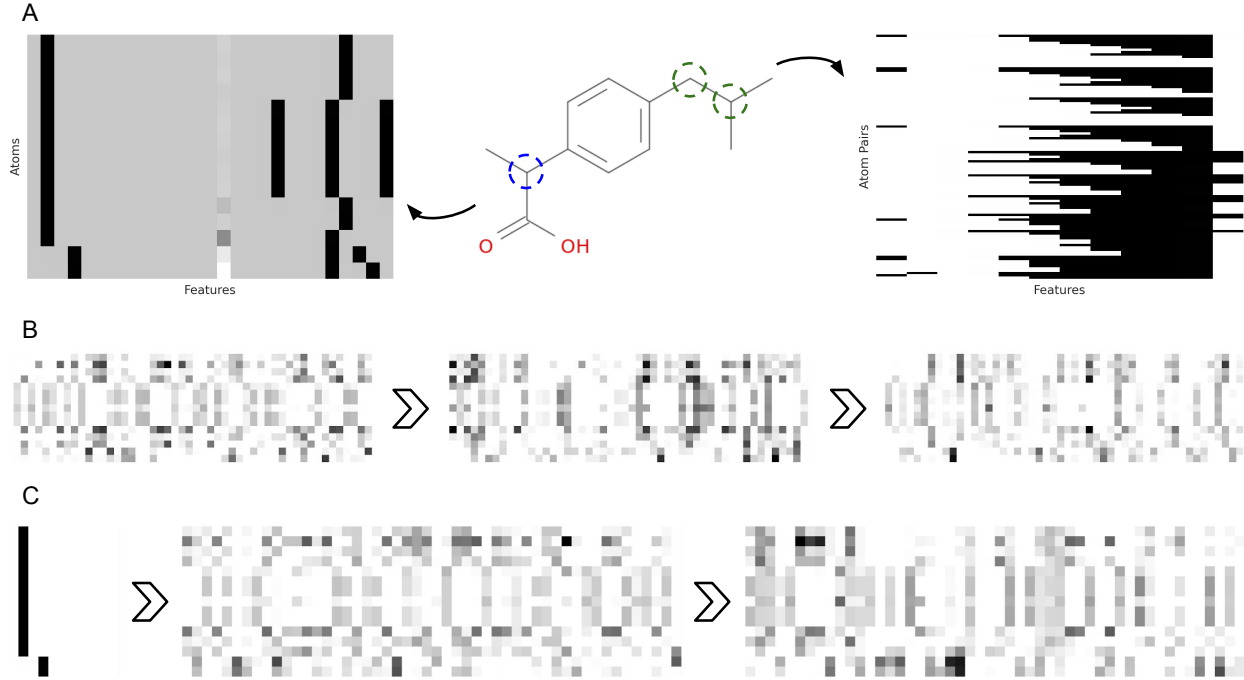


FIGURE 8: Graph convolution feature evolution. Atoms or pairs are displayed on the y -axis and the dimensions of the feature vectors are on the x -axis. (A) Conversion of the molecular graph for ibuprofen into atom and (unique) atom pair features. (B) Evolution of atom features after successive Weave modules in a graph convolution model with a W_3N_2 architecture and depth 50 convolutions in Weave modules. (C) Evolution of “simple” atom features (see Section 4.2) starting from initial encoding and progressing through the Weave modules of a W_2N_2 architecture.

RMS reductions on the PCBA datasets (Figure 10). These results are expected, since histograms capture the distribution of feature values rather than summarizing them in a single value.

4.3.3 Distance-dependent pair features

In the Weave module, atoms are informed about their chemical environment by mixing with pair features in the $P \rightarrow A$ operation. Recall that during this operation, pair features are combined for all pairs that contain a given atom, yielding a new representation for that atom. A critical parameter for this operation is the maximum distance (in bonds) allowed between the atoms of the pairs that are combined. If only adjacent atoms are combined, then the resulting atom features will reflect the local chemical environment. As an alternative to increasing the number of Weave modules, longer-range interactions can be captured by increasing the maximum atom pair distance. However, our implementation of the $P \rightarrow A$ operation uses a simple sum to combine pair features, which means that a lot of information (possibly including

every pair of atoms in the molecule) is being combined in a way that may prevent useful information from being available in later stages of the network.

Figure 11 and Figure A7 show the performance of several models with different maximum pair distances relative to a model that used only adjacent atom pairs (N_1). There is a slight decrease in performance with increasing pair distance, and N_∞ is clearly worse on the PCBA and Tox21 datasets. This trend suggests that the graph convolution models do not effectively handle or preserve the graph distance features for the initial atom pairs.

To further investigate the effect of distance information in Weave modules, we have begun experimenting with models that use distance-specific weights for operations involving pair features in order to maintain distance information explicitly throughout the network. However, these results are preliminary and were not included in this report.

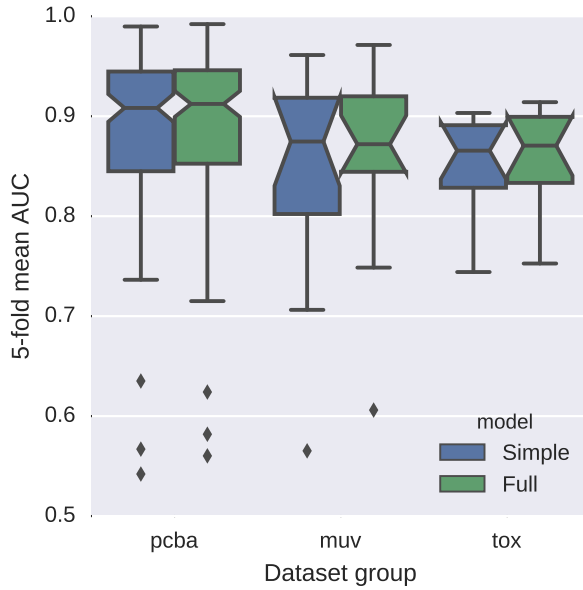


FIGURE 7: Comparison of models with “simple” and “full” input featurizations. The simple featurization only encodes atom type, bond type, and graph distance. The full featurization includes additional features such as aromaticity and hydrogen bonding propensity (see Section 3.3 for more details). Confidence intervals on box plot medians are computed as $\pm 1.57 \times \text{IQR}/\sqrt{N}$ (McGill et al., 1978).

5 Discussion

Graph convolutions are a deep learning architecture for learning directly from undirected graphs. In this work, we emphasize their application to small molecules—undirected graphs of atoms connected by bonds—for virtual screening. Starting from simple descriptions of atoms, bonds between atoms, and pairwise relationships in a molecular graph, we have demonstrated performance that is comparable to state of the art multitask models trained on traditional molecular fingerprint representations.

Flexibility is a highlight of the graph convolution architecture. Because we begin with a representation that encodes the complete molecular graph, graph convolution models are free to use any of the available information for the task at hand. In a sense, every possible molecular “fingerprint” is available to the model.

Our experiments with the adjustable parameters in graph convolution models suggest a relatively minor sensitivity to the number of Weave modules and the maximum distance between atom pairs. However, the

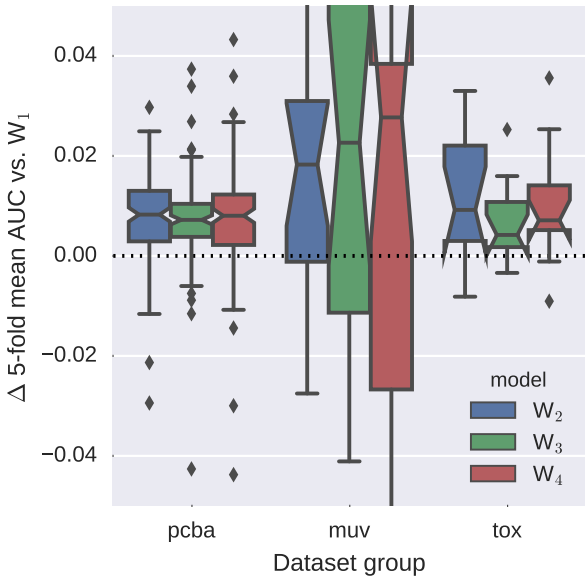


FIGURE 9: Comparison of models with different numbers of Weave modules with a model containing a single Weave module. All models used a maximum atom pair distance of two. The y -axis is cropped to emphasize differences near zero.

use of Gaussian histograms for reduction to molecule-level features is well supported, and there are trends suggesting that a model with two Weave modules and a maximum atom pair distance of 1 or 2 is a good starting point for further optimization. Remarkably, graph convolution models perform well with a “simple” input featurization containing only atom type, bond type, and graph distances—essentially the information available from looking at Figure 1.

Looking forward, graph convolutions present a “new hill to climb” in computational drug design and cheminformatics. To list just a few of the opportunities for further improvement: (1) additional optimization of model hyperparameters such as Weave module convolution depths, (2) fine-tuning of architectural decisions, such as the choice of reduction in the $P \rightarrow A$ operation (currently a sum, but perhaps a Gaussian histogram or distance-dependent function), (3) improvements in memory usage and training performance, such as not handling all pairs of atoms or implementing more efficient versions of Weave module operations. With these and other optimizations, we anticipate that graph convolutions will exceed the performance of the best available fingerprint representations.

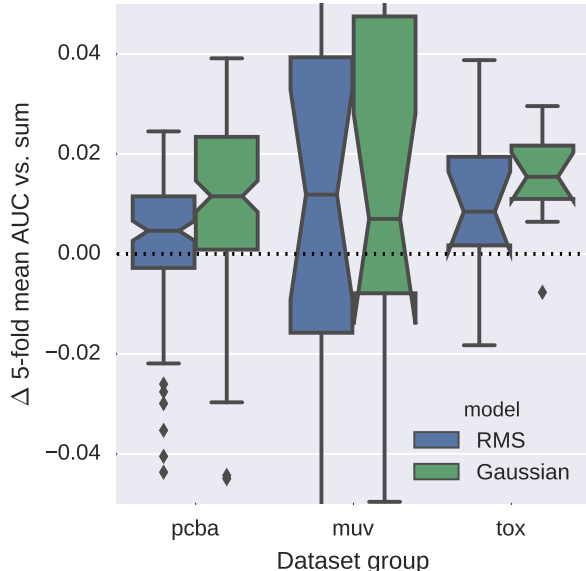


FIGURE 10: Comparison of root-mean-square (RMS) and Gaussian histogram reductions *vs.* sum reduction. The *y*-axis reports difference in 5-fold mean AUC relative to sum reduction. All models used two Weave modules and a maximum atom pair distance of two. The *y*-axis is cropped to emphasize differences near zero.

Finally, we note that much (or most) of the information required to represent biological systems and the interactions responsible for small molecule activity is not encapsulated in the molecular graph. Biology takes place in a three-dimensional world, and can be more sensitive to shape, electrostatics, quantum effects, and other properties that emerge from the molecular graph than the structure of the graph itself (see, *e.g.*, Nicholls and Grant (2005); Böhm et al. (2004), and related literature on “scaffold hopping”). Additionally, most small molecules exhibit 3D conformational flexibility that our graph representation does not even attempt to describe. The extension of deep learning methods (including graph convolutions) to three-dimensional biology is an active area of research (*e.g.*, Wallach et al. (2015)) that requires special attention to the added complexities of multiple-instance learning in a relatively small-data regime.

Acknowledgments

We thank Bharath Ramsundar, Brian Goldman, and Robert McGibbon for helpful discussion. We also ac-

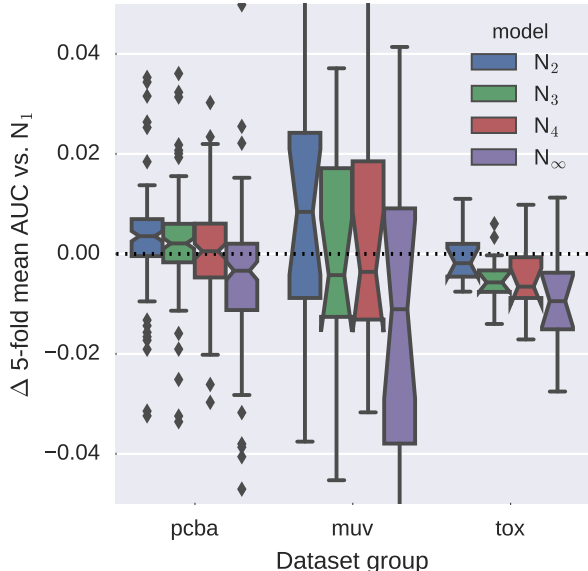


FIGURE 11: Comparison of models with different maximum atom pair distances to a model with a maximum pair distance of one (bonded atoms). All models have two Weave modules. The *y*-axis is cropped to emphasize differences near zero.

knowledge Manjunath Kudlur, Derek Murray, and Rajat Monga for assistance with TensorFlow. S.K. was supported by internships at Google Inc. and Vertex Pharmaceuticals Inc.

References

Martin Abadi, Ashish Agarwal, Paul Barham, Eugene Brevdo, Zhifeng Chen, Craig Citro, Greg S Corrado, Andy Davis, Jeffrey Dean, Matthieu Devin, et al. TensorFlow: Large-scale machine learning on heterogeneous systems. *Software available from tensorflow.org*, 2015.

Pedro J Ballester and W Graham Richards. Ultrafast shape recognition to search compound databases for similar molecular shapes. *Journal of computational chemistry*, 28(10):1711–1723, 2007.

Hans-Joachim Böhm, Alexander Flohr, and Martin Stahl. Scaffold hopping. *Drug Discovery Today: Technologies*, 1(3):217–224, 2004.

Hans Briem and Uta F Lessel. In vitro and in silico affinity fingerprints: Finding similarities beyond

structural classes. *Perspectives in Drug Discovery and Design*, 20(1):231–244, 2000.

Joan Bruna, Wojciech Zaremba, Arthur Szlam, and Yann LeCun. Spectral networks and locally connected networks on graphs. *arXiv preprint arXiv:1312.6203*, 2013.

Raymond E Carhart, Dennis H Smith, and R Venkataraghavan. Atom pairs as molecular features in structure-activity studies: definition and applications. *Journal of Chemical Information and Computer Sciences*, 25(2):64–73, 1985.

Sander Dieleman. Classifying plankton with deep neural networks. <http://benanne.github.io>, March 17, 2015.

John Duchi, Elad Hazan, and Yoram Singer. Adaptive subgradient methods for online learning and stochastic optimization. *The Journal of Machine Learning Research*, 12:2121–2159, 2011.

David K. Duvenaud, Dougal Maclaurin, Jorge Aguilera-Iparraguirre, Rafael Gómez-Bombarelli, Timothy Hirzel, Alán Aspuru-Guzik, and Ryan P. Adams. Convolutional networks on graphs for learning molecular fingerprints. *CoRR*, abs/1509.09292, 2015. URL <http://arxiv.org/abs/1509.09292>.

Johann Gasteiger and Mario Marsili. Iterative partial equalization of orbital electronegativity—a rapid access to atomic charges. *Tetrahedron*, 36(22): 3219–3228, 1980.

GraphSim Toolkit, OpenEye Scientific Software, Inc., Santa Fe, NM, USA. Version 2.2.2. <http://www.eyesopen.com>.

Dragos Horvath. Pharmacophore-based virtual screening. In *Chemoinformatics and computational chemical biology*, pages 261–298. Springer, 2011.

Ruili Huang, Menghang Xia, Dac-Trung Nguyen, Tongan Zhao, Srilatha Sakamuru, Jinghua Zhao, Sampada A Shahane, Anna Rossoshek, and Anton Simeonov. Tox21challenge to build predictive models of nuclear receptor and stress response pathways as mediated by exposure to environmental chemicals and drugs. *Frontiers in Environmental Science*, 3:85, 2015.

Sergey Ioffe and Christian Szegedy. Batch normalization: Accelerating deep network training by reducing internal covariate shift. *arXiv preprint arXiv:1502.03167*, 2015.

Michael J Keiser, Bryan L Roth, Blaine N Armbruster, Paul Ernsberger, John J Irwin, and Brian K Shoichet. Relating protein pharmacology by ligand chemistry. *Nature biotechnology*, 25(2): 197–206, 2007.

Greg Landrum. RDKit: Open-source cheminformatics; <http://www.rdkit.org>. URL <http://www.rdkit.org>.

Yann LeCun, Yoshua Bengio, and Geoffrey Hinton. Deep learning. *Nature*, 521(7553):436–444, 2015.

Alessandro Lusci, Gianluca Pollastri, and Pierre Baldi. Deep architectures and deep learning in chemoinformatics: the prediction of aqueous solubility for drug-like molecules. *Journal of chemical information and modeling*, 53(7):1563–1575, 2013.

Junshui Ma, Robert P. Sheridan, Andy Liaw, George E. Dahl, and Vladimir Svetnik. Deep neural nets as a method for quantitative structure–activity relationships. *Journal of Chemical Information and Modeling*, 55(2):263–274, 2015. doi: 10.1021/ci500747n. URL <http://dx.doi.org/10.1021/ci500747n>. PMID: 25635324.

Jonathan Masci, Davide Boscaini, Michael M. Bronstein, and Pierre Vandergheynst. Shapenet: Convolutional neural networks on non-euclidean manifolds. *CoRR*, abs/1501.06297, 2015. URL <http://arxiv.org/abs/1501.06297>.

Robert McGill, John W Tukey, and Wayne A Larsen. Variations of box plots. *The American Statistician*, 32(1):12–16, 1978.

Christian Merkwirth and Thomas Lengauer. Automatic generation of complementary descriptors with molecular graph networks. *Journal of chemical information and modeling*, 45(5):1159–1168, 2005.

Alessio Micheli. Neural network for graphs: A contextual constructive approach. *Trans. Neur. Netw.*, 20(3):498–511, March 2009. ISSN 1045-9227. doi: 10.1109/TNN.2008.2010350. URL <http://dx.doi.org/10.1109/TNN.2008.2010350>.

Steven W Muchmore, Andrew J Souers, and Irini Akritopoulou-Zanze. The use of three-dimensional shape and electrostatic similarity searching in the

identification of a melanin-concentrating hormone receptor 1 antagonist. *Chemical biology & drug design*, 67(2):174–176, 2006.

Michael M Mysinger, Michael Carchia, John J Irwin, and Brian K Shoichet. Directory of useful decoys, enhanced (dud-e): better ligands and decoys for better benchmarking. *Journal of medicinal chemistry*, 55(14):6582–6594, 2012.

Anthony Nicholls and J Andrew Grant. Molecular shape and electrostatics in the encoding of relevant chemical information. *Journal of computer-aided molecular design*, 19(9-10):661–686, 2005.

Fabian Pedregosa, Gaël Varoquaux, Alexandre Gramfort, Vincent Michel, Bertrand Thirion, Olivier Grisel, Mathieu Blondel, Peter Prettenhofer, Ron Weiss, Vincent Dubourg, et al. Scikit-learn: Machine learning in python. *The Journal of Machine Learning Research*, 12:2825–2830, 2011.

Paula M Petrone, Benjamin Simms, Florian Nigsch, Eugen Lounkine, Peter Kutchukian, Allen Cornett, Zhan Deng, John W Davies, Jeremy L Jenkins, and Meir Glick. Rethinking molecular similarity: comparing compounds on the basis of biological activity. *ACS chemical biology*, 7(8):1399–1409, 2012.

Bharath Ramsundar, Steven Kearnes, Patrick Riley, Dale Webster, David Konerding, and Vijay Pande. Massively multitask networks for drug discovery. *arXiv preprint arXiv:1502.02072*, 2015.

David Rogers and Mathew Hahn. Extended-connectivity fingerprints. *Journal of chemical information and modeling*, 50(5):742–754, 2010.

Sebastian G Rohrer and Knut Baumann. Maximum unbiased validation (muv) data sets for virtual screening based on pubchem bioactivity data. *Journal of chemical information and modeling*, 49(2):169–184, 2009.

Thomas S Rush, J Andrew Grant, Lidia Mosyak, and Anthony Nicholls. A shape-based 3-d scaffold hopping method and its application to a bacterial protein-protein interaction. *Journal of medicinal chemistry*, 48(5):1489–1495, 2005.

F. Scarselli, M. Gori, A. C. Tsoi, M. Hagenbuchner, and G. Monfardini. The graph neural network model. *IEEE Trans Neural Netw*, 20(1):61–80, Jan 2009.

Skipper Seabold and Josef Perktold. Statsmodels: Econometric and statistical modeling with python. In *Proceedings of the 9th Python in Science Conference*, pages 57–61, 2010.

Nitish Srivastava, Geoffrey Hinton, Alex Krizhevsky, Ilya Sutskever, and Ruslan Salakhutdinov. Dropout: A simple way to prevent neural networks from overfitting. *The Journal of Machine Learning Research*, 15(1):1929–1958, 2014.

Christian Szegedy, Wei Liu, Yangqing Jia, Pierre Sermanet, Scott Reed, Dragomir Anguelov, Dumitru Erhan, Vincent Vanhoucke, and Andrew Rabinovich. Going deeper with convolutions. In *CVPR 2015*, 2015. URL <http://arxiv.org/abs/1409.4842>.

Roberto Todeschini and Viviana Consonni. *Molecular Descriptors for Chemoinformatics, Volume 41 (2 Volume Set)*, volume 41. John Wiley & Sons, 2009.

Thomas Unterthiner, Andreas Mayr, GÃ¼nter Klambauer, and Sepp Hochreiter. Toxicity prediction using deep learning. *arXiv preprint arXiv:1503.01445*, 2015.

Izhar Wallach, Michael Dzamba, and Abraham Heifets. Atomnet: A deep convolutional neural network for bioactivity prediction in structure-based drug discovery. *arXiv preprint arXiv:1510.02855*, 2015.

Yanli Wang, Jewen Xiao, Tugba O Suzek, Jian Zhang, Jiyao Wang, Zhigang Zhou, Lianyi Han, Karen Karapetyan, Svetlana Dracheva, Benjamin A Shoemaker, et al. Pubchem’s bioassay database. *Nucleic acids research*, 40(D1):D400–D412, 2012.

Lotfi A Zadeh. Fuzzy sets. *Information and control*, 8(3):338–353, 1965.

APPENDIX

A Model comparison

The following figures are box plot representations of the data summarized in Table 4, organized by dataset group. We provide (a) box plots for absolute 5-fold mean AUC scores for each model and (b) difference box plots showing differences in 5-fold mean AUC scores against the Pyramidal (2000, 100) MTNN (PMTNN) or Random Forest (RF) baseline model. The difference box plots are visual analogs of the sign test confidence intervals reported in Table 4. Note, however, that the confidence intervals on box plot medians (calculated as $\pm 1.57 \times \text{IQR}/\sqrt{N}$ (McGill et al., 1978)) do not necessarily correspond to the sign test confidence intervals.

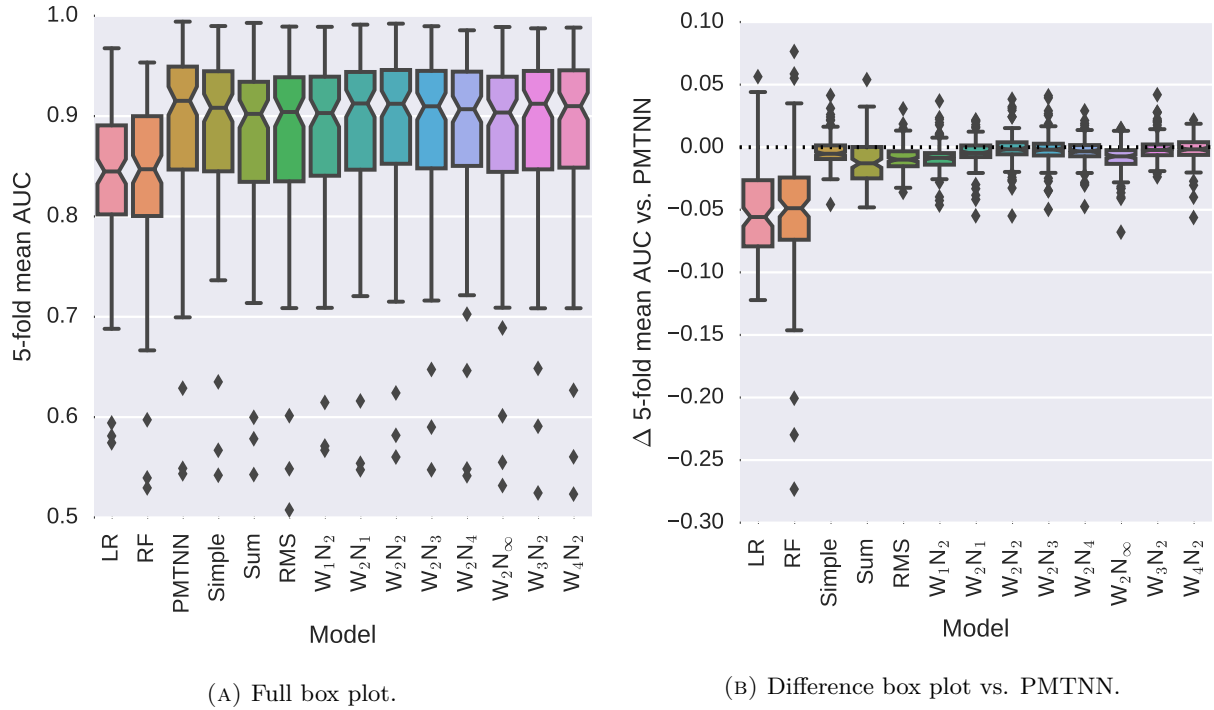


FIGURE A1: Model performance on PCBA datasets.

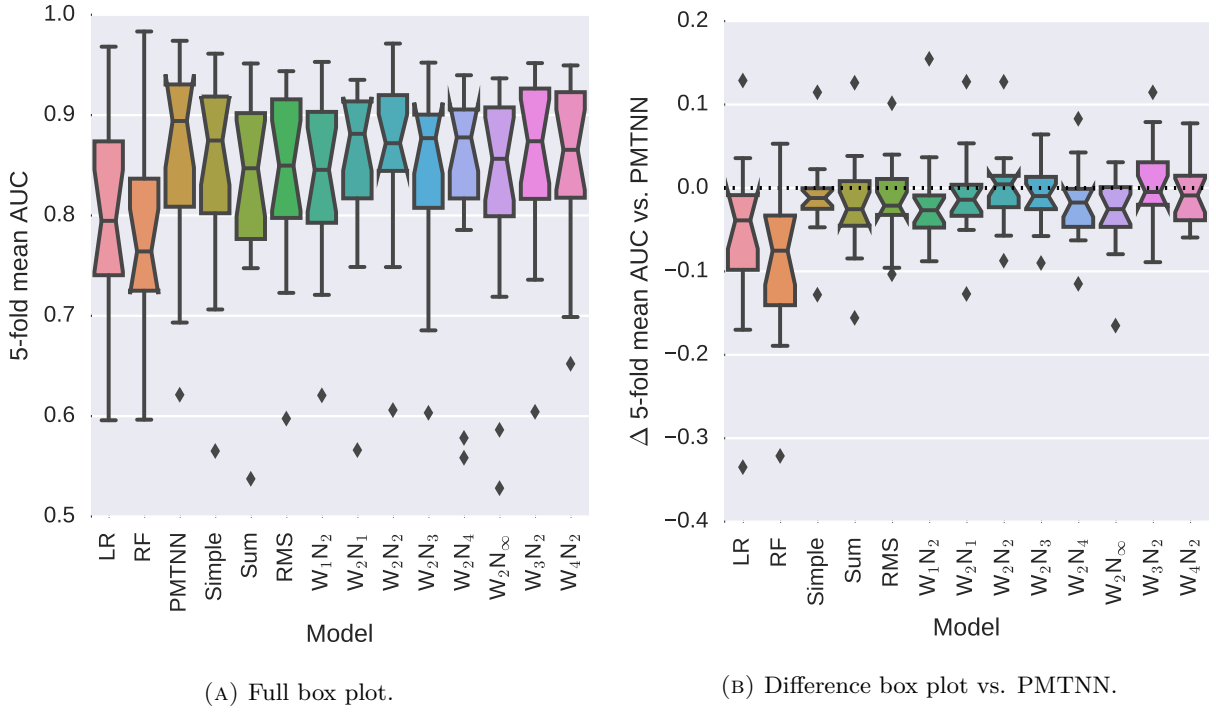


FIGURE A2: Model performance on MUV datasets.

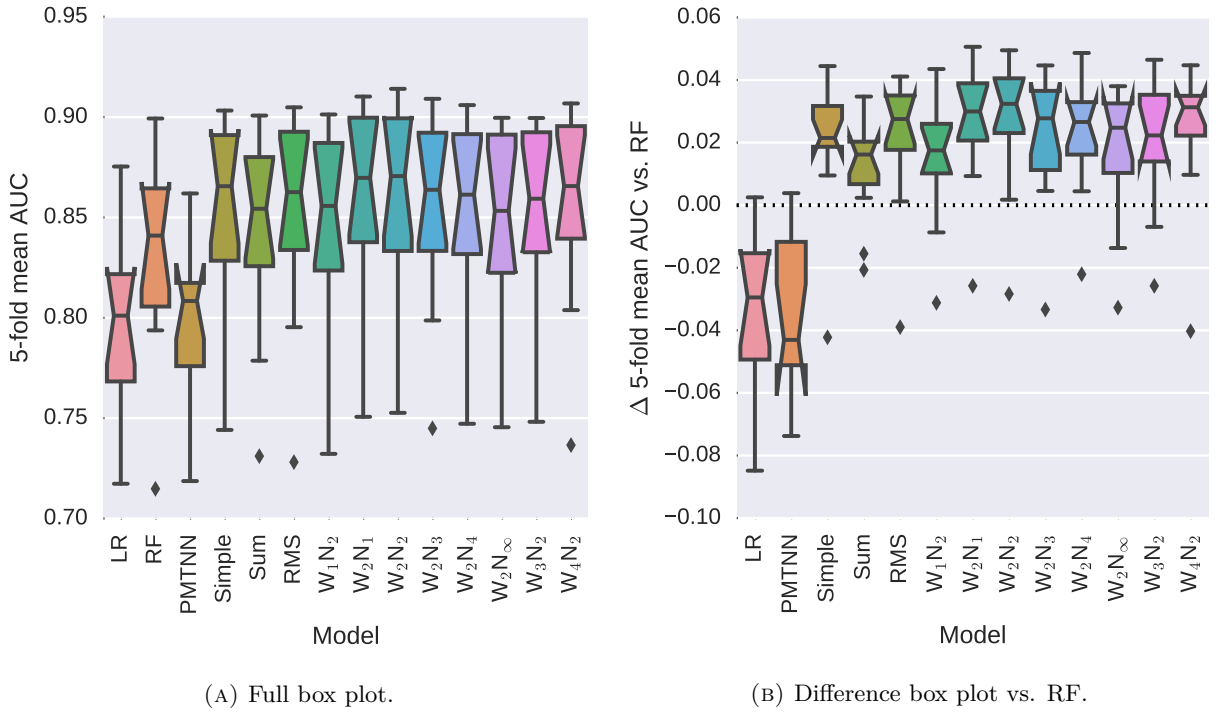


FIGURE A3: Model performance on Tox21 datasets.

B Input featurization

For each of the experiments described in Section 4.2, we provide figures showing (a) box plots for absolute 5-fold mean AUC scores for each model and (b) difference box plots showing differences in 5-fold mean AUC scores against a baseline model (without any y -axis cropping).

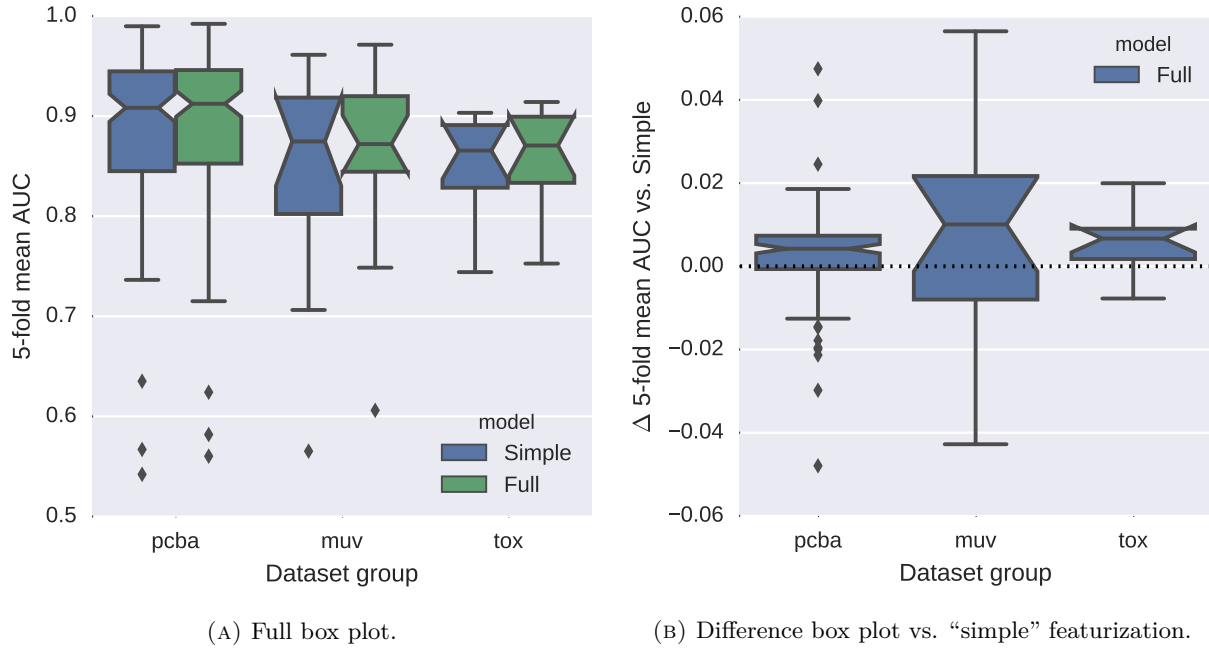


FIGURE A4: Comparison of models with “simple” and “full” input featurizations.

C Hyperparameter sensitivity

For each of the experiments described in Section 4.3, we provide figures showing (a) box plots for absolute 5-fold mean AUC scores for each model and (b) difference box plots showing differences in 5-fold mean AUC scores against a baseline model (without any y -axis cropping).

C.1 Number of Weave modules

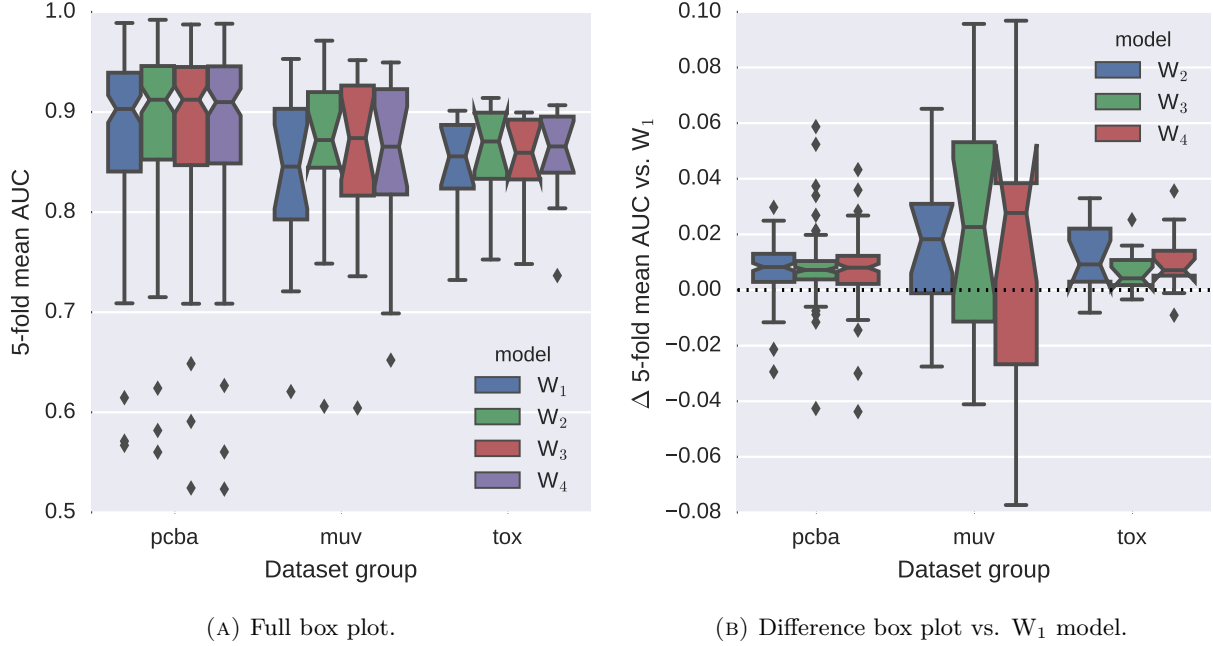


FIGURE A5: Comparison of models with different numbers of Weave modules.

C.2 Alternative feature reductions

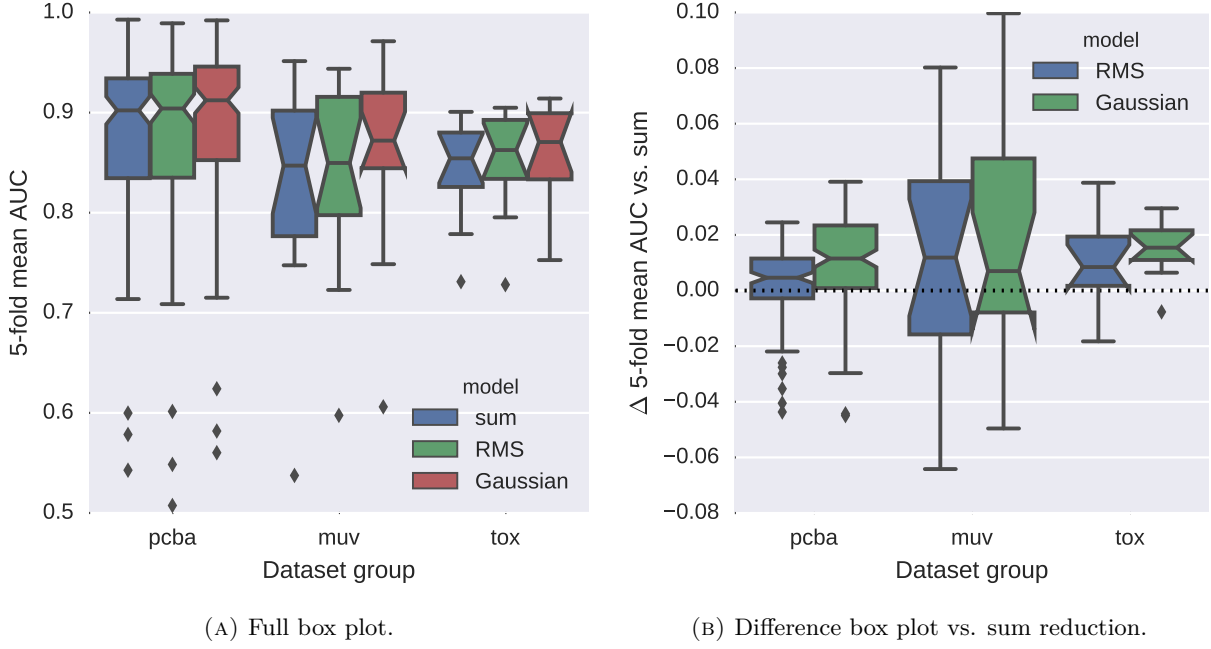


FIGURE A6: Comparison of models with different feature reduction methods.

C.3 Distance-dependent pair features

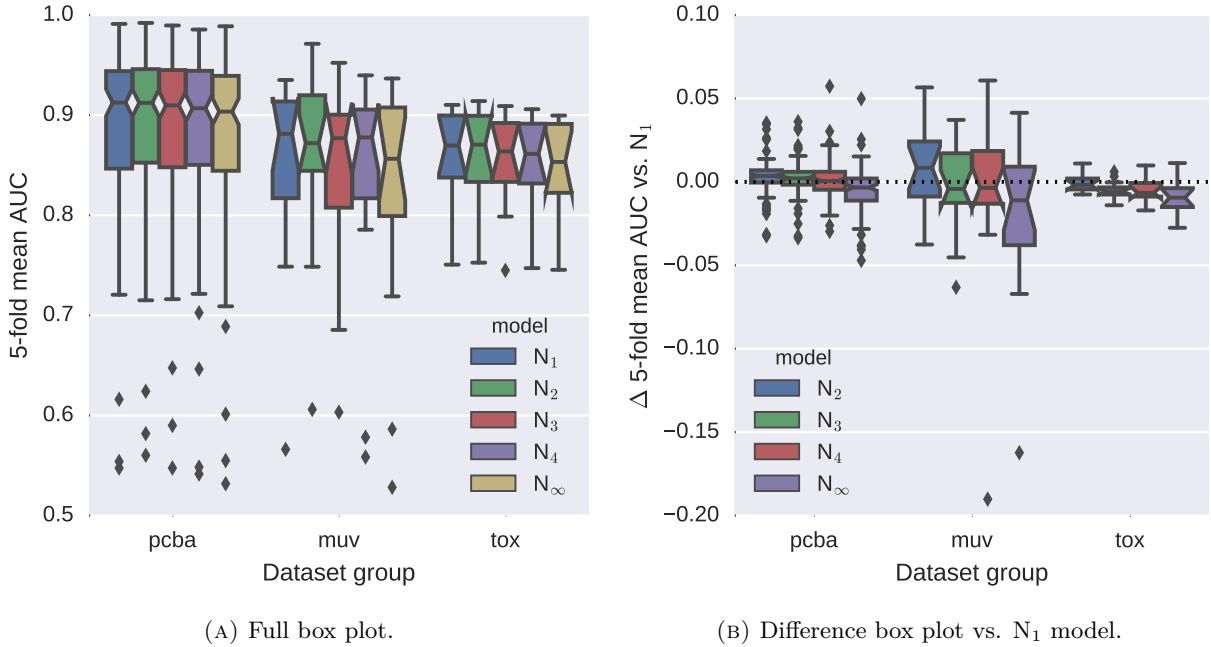


FIGURE A7: Comparison of models with different maximum atom pair distances.

D Atom pair feature evolution

Figure 8 showed the evolution of atom features at different stages of a graph convolution model (after subsequent Weave modules). The following figures show the evolution of atom pair features from the same models, using both the “full” and “simple” input featurization. As in Figure 8, the initial pair features describe ibuprofen. Most of the initial featurization describes the graph distance between the atoms in the pair (see Table 3). There are many blank rows since pairs separated by more than the maximum atom pair distance are masked. Note that only unique pairs are represented (*i.e.*, (a, b) but not (b, a)). As the pair features move through the graph convolution network, it can be seen that identical initial featurizations diverge due to mixing with atom features in Weave modules.

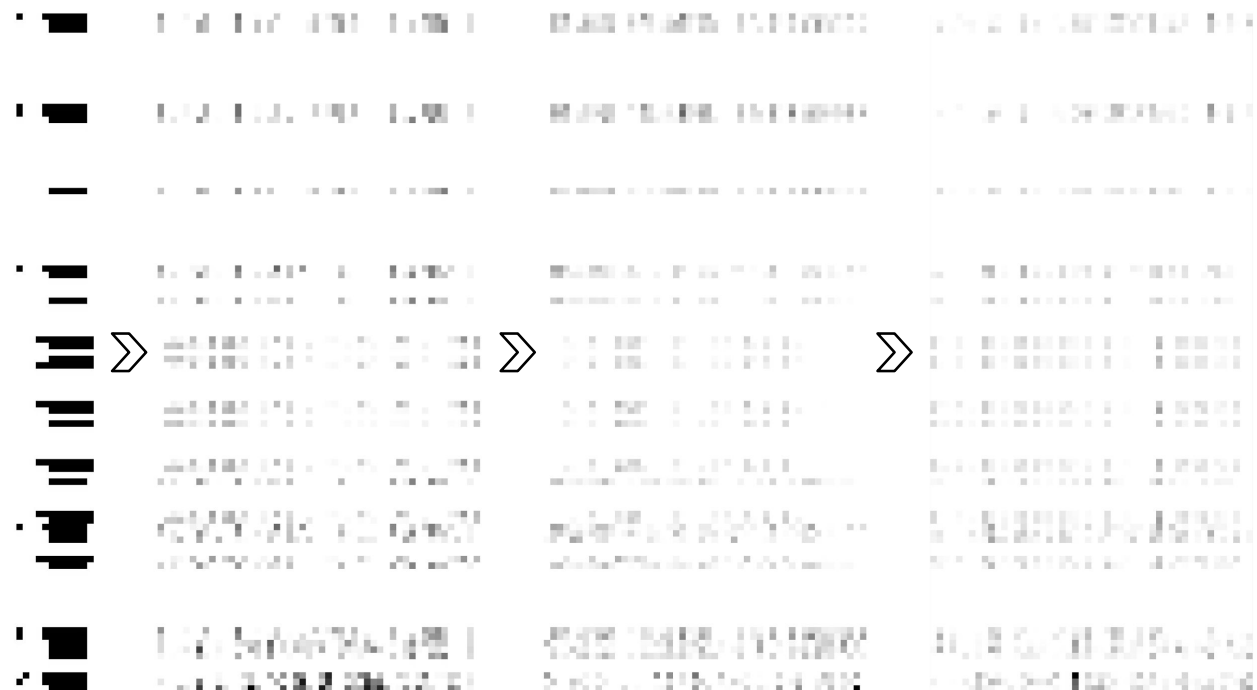


FIGURE A8: Graph convolution atom pair feature evolution using the “full” featurization in a W_3N_2 architecture. Unique atom pairs are on the y -axis (one atom pair per row). Initial pair features are shown on the left, with whitespace separating subsequent Weave module outputs.

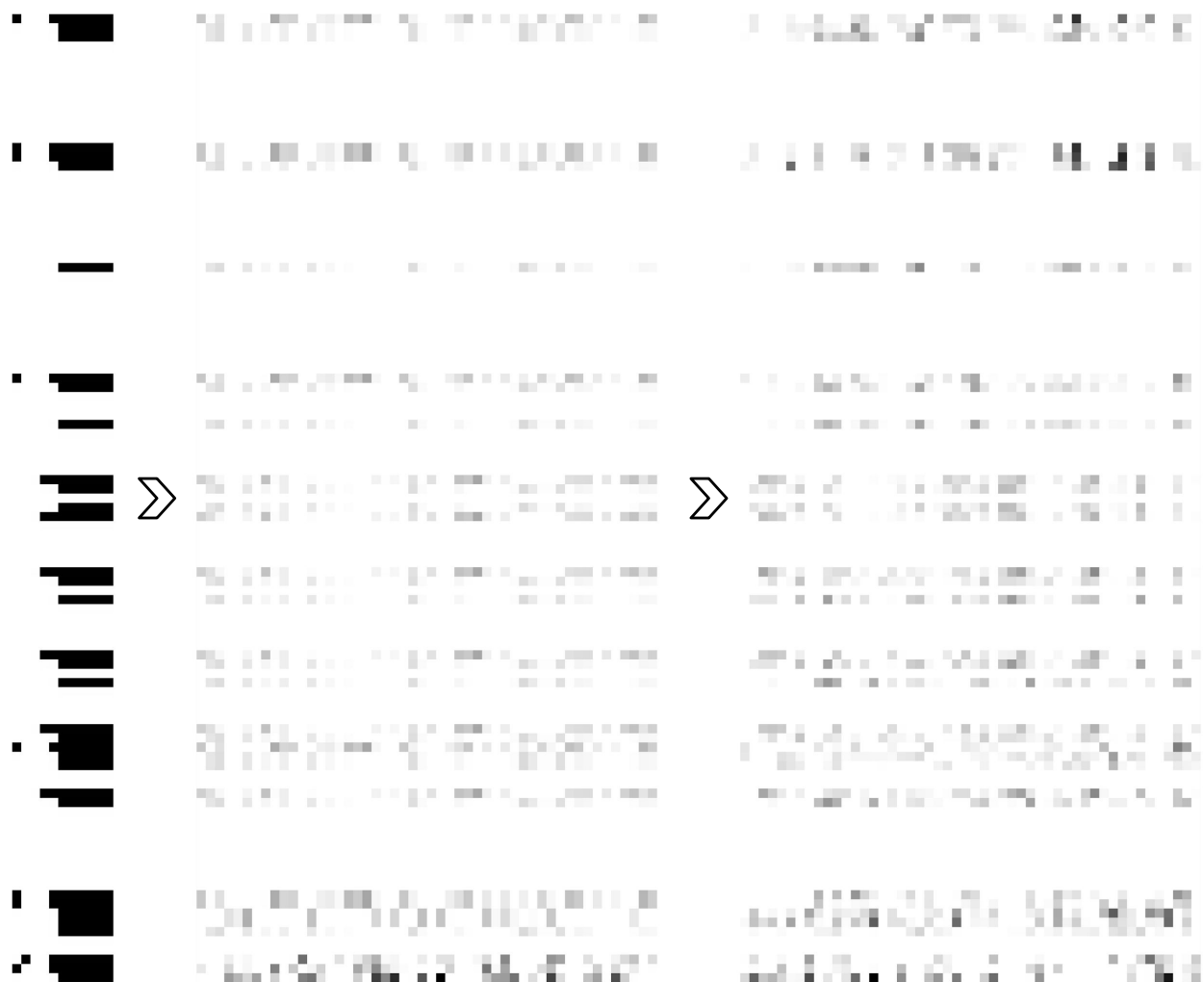


FIGURE A9: Graph convolution atom pair feature evolution using the “simple” featurization in a W_2N_2 architecture. Unique atom pairs are on the y -axis (one atom pair per row). Initial pair features are shown on the left, with whitespace separating subsequent Weave module outputs.

E Gaussian histogram membership functions

TABLE A1: Gaussian membership functions.

| Mean | Variance |
|--------|----------|
| -1.645 | .080 |
| -1.080 | .029 |
| -.739 | .018 |
| -.468 | .014 |
| -.228 | .013 |
| .000 | .013 |
| .228 | .013 |
| .468 | .014 |
| .739 | .018 |
| 1.080 | .029 |
| 1.645 | .080 |

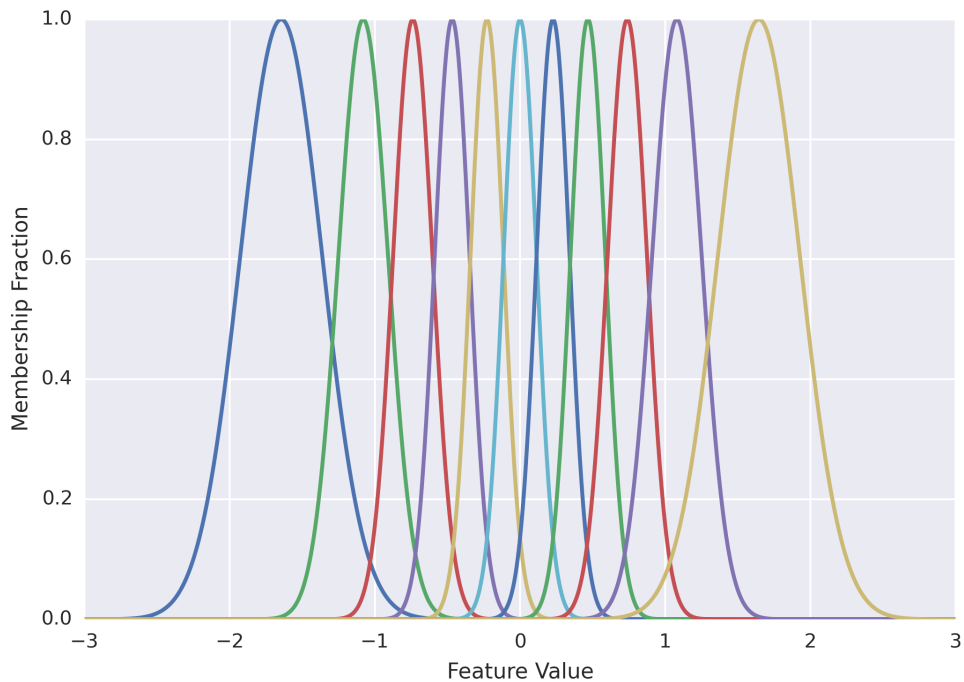


FIGURE A10: Visualization of the Gaussian membership functions.

References

Robert McGill, John W Tukey, and Wayne A Larsen. Variations of box plots. *The American Statistician*, 32(1):12–16, 1978.